



Effect of erosion rate and particle mass loading on separation efficiency of square cyclone by considering gas temperature

Ebrahim Hosseini¹ · Mohammad Amin Atarzadeh¹ · Mehdi Shekarzadeh¹

Received: 26 January 2022 / Accepted: 29 July 2022 / Published online: 17 August 2022
© The Author(s), under exclusive licence to The Brazilian Society of Mechanical Sciences and Engineering 2022

Abstract

Although it is commonly thought that particle mass loading (PML) may have a considerable impact on fluid flow in cyclone separators, the specific effect can be confusing due to a lack of fundamental understanding of the working principles. The problem was addressed in this study by using the Computational Fluid Dynamics technique to numerically analyze the PML effect of different sizes on the flow within the square cyclone separator. This type of cyclone is an effective cleaning mechanism for high-temperature gases in a Circulating Fluidized Bed boiler. Therefore, it is also critical to investigate the effect of PML on gas flow at low and high temperatures, which has yet to be taken into account in the literature. The Eulerian–Lagrangian approach was adopted for solving the Unsteady Reynolds-Averaged Navier–Stokes equations to model particle flow. To model velocity fluctuations, the Discrete Random Walk was adopted. Furthermore, the Det Norske Veritas erosion model was utilized for predicting the erosion rate caused by solid particles. The results revealed that as the PML raised the improved bigger particles sweeping impact forced the smaller particles to move toward the wall region and increased the concentration of particles at the wall region. As the PML raised from 6.9 to 41.7 g/m³, the concentration of particles at the bottom of the square cyclone grew up to 11 times. As the gas tangential velocity increased with PML, more particles collected at bottom of the conical section and stayed there for an extended period, increasing the chances of their separation. In addition, it was concluded that with the increase in inlet velocity and PML, the erosion rate enhanced. Roughly four times enhancement of maximum erosion rate was predicted with PML = 41.7 g/m³.

Keywords Square cyclone · Erosion · Particle mass loading · CFD

List of symbols

C_D	Drag coefficient
R_{ij}	Reynolds stress tensor
ν	Kinematic viscosity (m ² /s)
u_{pi}	Particle velocity (m/s)
K	Fluctuating kinetic energy (m ² /s ²)
t	Time (s)
u_i	Gas velocity (m/s)
ϵ	Turbulence dissipation rate (m ² /s ³)
g_i	Gravitational acceleration (m/s ²)
v	Velocity (m/s)
P_f	Fluctuating energy production (m ² /s ³)
d_p	Particle diameter (μm)

μ	Dynamic viscosity (kg/ms)
Re_p	Relative Reynolds number
ρ	Density (kg/m ³)
P	Pressure (Pa)
ρ_p	Particle density (kg/m ³)

1 Introduction

Cyclones are now widely utilized as a vital tool in the separation process in a variety of industries. Filters, electrostatic separators, and sediment separators compete with cyclones. Cyclones, on the other hand, are less expensive to develop and operate than other solid–gas separators. Because of these characteristics, they are widely used in different industrial areas, including oil, gas, petrochemicals, refineries, manufacturing, food industries, and so on. Cyclones are remarkably applied in the control of air pollution to separate particulate gas mixtures and are employed in the industry. The advantages of this device in different industries are its

Technical Editor: Erick Franklin.

✉ Ebrahim Hosseini
ebrahim.2019.hosseini@gmail.com

¹ Department of Mechanical Engineering, Islamic Azad University, Ahvaz Branch, Ahvaz, Iran

relative simplicity of construction, low operating cost, and adaptation to harsh working conditions. Today, a gas cyclone is the major particle removal tool in the fields of science and engineering. Gas cyclones are commonly popular and effective separation devices that remove particles from a gas stream using centrifugal force [1]. Cyclones are often categorized as square or conventional [2–5]. Cyclones are also utilized as an integral part of a Circulating Fluidized Bed (CFB) to separate solids derived from flue gases. The conventional rounded cyclone was extensively utilized in industries for CFB boilers. CFB boilers are widely used in the power generating industry providing clean coal combustion. The large body of typical cyclones became a significant disadvantage with the growth of CFB boilers owing to the thick refractory wall needing a lengthy start-up time. The square gas cyclone can be used as an option to effectively deal with these limitations. This kind of cyclone offers several benefits over the conventional circular cyclone, including design simplicity, and faster start-stop time [6–8]. A square cyclone is smaller than a cylindrical cyclone, the enhanced membrane wall arrangement minimizes the volume of the multi-phase components as well as the start and stop time, and it is effectively merged with the boiler [7, 9]. However, this sort of gas cyclone had a low separation efficiency. Few studies have attempted to investigate the particle separation efficiency of square cyclones and their turbulent characteristics. For example, Venkatesh et al. [6] experimentally and numerically considered three square cyclones which were connected in the series arrangement. Their experimental work was done to evaluate collection efficiency and pressure drop. Their series arrangement cyclone's collecting efficiency is predicted to be 61%. The series arrangement layout reduces the pressure drop to 14.3%. Moreover, the flow pattern outcome is more consistent with the experimental data. Safikhani et al. [10] numerically analyzed particle separation efficiency of small square and round (traditional) cyclones. They reported that the pressure drop in square gas cyclone is less than that in cylindrical one. In a study, Fatahian et al. [11] demonstrated that incorporating a laminarizer into a conventional or square cyclone improves particle separation efficiency. Fatahian et al. [12] computationally assessed the effect of dual inverse cones on the characteristics of the cyclone separator. Their research confirmed that the dual inverse cone raises pressure drop and collection efficiency marginally in the square cyclone.

The effect of PML on cyclone performance, particularly square cyclone performance, has rarely been studied. When PML exceeds 500 g/m^3 , the pressure drop across the cyclone reduces and the gas tangential velocity decreases [13–15]. The cyclone separation efficiency rises with PML due to the sweeping impacts of bigger particles and particle agglomeration within the cyclone body [13]. As the PML is between 0 and 130 g/m^3 , the particle separation efficiency

improves as the PML increases [16, 17]. Derksen et al. [18] considered the impact of PML on the flow patterns within the cyclone numerically. The presence of solid particles reduces the swirl intensity of the gas cyclone. Besides that, the turbulence of the gas flow is remarkably damped. Huang et al. [17] investigated the influence of PML on cyclone performance experimentally and numerically. They concluded that increasing the PML raised the particles near the wall. Experiment findings showed that higher PML enhanced separation efficiency when the inlet gas velocity was low. Wan et al. [19] used the Lagrangian technique to quantitatively assess the solid concentrations of different particle sizes in a cyclone separator. They revealed that the presence of solid particles greatly altered the gas flow field and the swirl was minimized as the solid loading increased.

Another significant phenomenon in cyclone separators is erosion at the walls caused by the suspension of solid particles in fluid flow. In general, one of the key challenges in the transfer of fluid–solid flows is solid particle erosion [20]. The use of CFD tools to solve complex engineering problems is a robust methodology that may be utilized to analyze the erosion phenomena, especially given the high cost and time required to conduct physical experiments. The Lagrange approach is mostly used in this sort of simulation because it allows the movement of a single particle to be evaluated. As a result, critical pieces of information on particle characteristics including velocity, impact angle, and particle concentration may be provided [21]. The Euler–Lagrange technique has been utilized in published research to forecast erosion in elbows [22], valves [23], pipes [24], and gas cyclones [25–27]. Sedrez et al. [21] conducted an experimental and computational study of particle wear on cylindrical and conical portions of the cyclone. They reported that augmenting the gas velocity and solids loading accelerated erosion and increased pressure drop. Parvaz et al. [28] conducted CFD simulations of a gas cyclone to show that the erosion rate decreases as the restitution coefficient increases. The effect of wall roughness of cyclones on erosion rate and performance of gas cyclones was investigated using CFD in the study of Foroozesh et al. [29]. The findings of their investigation demonstrated that the roughness of the cyclone wall had a substantial impact on airflow behavior and cyclone performance. It was also revealed that solid loading and inflow gas velocity had a major effect on erosion rate, even more than particle size. Dehdarinejad and Bayareh [20] investigated the effect of nonuniform surface roughness on the improvement and erosion rate of a Staimand gas cyclone. Nonuniform roughness is addressed for the cylindrical component, cone, and vortex finder of the cyclone. They demonstrated that the erosion rate of cyclones with nonuniformly roughened walls is lower than that of smooth-walled cyclones including all mass loading conditions.

The presented literature survey revealed that, although some studies have been done in the area of PML on cyclone performance, a fundamental understanding of particle concentration inside the cyclone is still in its early evaluation and analytical modeling steps. More emphasis was put on cyclone design and parametric analysis than on particle behavior and gas flow characteristics. Following the influences on cyclone performance, particularly square cyclone separator, there is quite limited experimental and numerical data for PML. This study attempts to address this gap in the literature by providing a quantitative analysis of particle concentration and conducting a comprehensive assessment of PML and its impact on cyclone separation efficiency. Finally, the effect of particle-induced erosion on different inlet velocities, and various PMLs were studied.

2 Numerical modeling

2.1 Model description

Figure 1 a, b shows a schematic perspective and 3D model of a square cyclone according to the experimental results of Su and Mao [30]. Also, Table 1 depicts the square cyclone's geometrical dimensions. In this study, the commercial program ANSYS-ICEM CFD is utilized to create a structural hexahedral grid, which is shown in Fig. 1c.

Fig. 1 Schematic perspective of **a** geometrical model, **b** 3D model, **c** structural grid

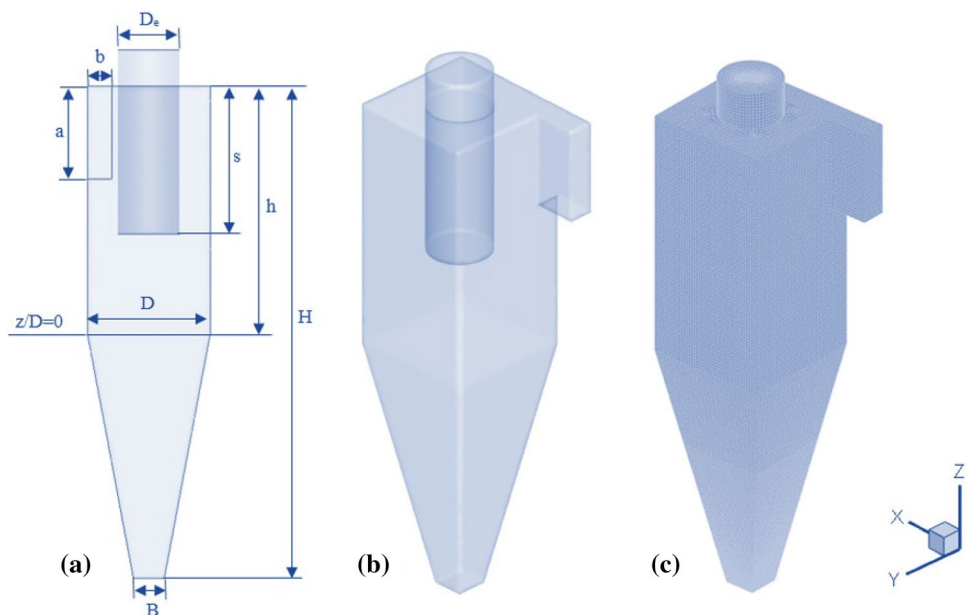


Table 1 Dimensions of cyclone ($D = 200$ mm)

Dimensions	D_e/D	a/D	b/D	s/D	h/D	H/D	B/D
Cyclone separator	0.5	0.75	0.2	1.2	2	4	0.25

2.2 Governing equations

A 3D CFD simulation was done to simulate the flow within the cyclone. The URANS equations for the incompressible flow are as follows [31]:

$$\frac{\partial \bar{u}_i}{\partial x_i} = 0 \tag{1}$$

$$\frac{\partial \bar{u}_i}{\partial t} + \bar{u}_j \frac{\partial \bar{u}_i}{\partial x_j} = -\frac{1}{\rho} \frac{\partial \bar{P}}{\partial x_i} + \nu \frac{\partial^2 \bar{u}_i}{\partial x_j \partial x_j} - \frac{\partial}{\partial x_j} R_{ij} \tag{2}$$

where \bar{u}_i represents the mean velocity, x_i indicates the spatial position, ρ is the gas density, and ν corresponds to the gas kinematic viscosity. Here \bar{P} shows the mean pressure and $R_{ij} = \overline{u'_i u'_j}$ is the Reynolds stress tensor, where denote the i th fluctuating velocity component.

According to the previous studies, only the Reynolds Stress Turbulence Model (RSTM) and Large Eddy Simulation (LES) are widely recognized to accurately capture the major aspects of complex swirling flows of gas cyclones [32–34]. The LES method offers more accurate findings than the RSTM for estimating flow within cyclones, but it has a higher computational cost. Hence, the RSTM [35] was utilized to analyze turbulent airflow in a square cyclone in the present CFD simulation. The RSTM computes differential transport equations for evaluating turbulence stress

components, with the following turbulence production terms [35]:

$$\frac{\partial}{\partial t} R_{ij} + \bar{u}_k \frac{\partial}{\partial x_k} R_{ij} = \frac{\partial}{\partial x_k} \left(\frac{\nu_t}{\sigma^k} \frac{\partial}{\partial x_k} R_{ij} \right) - \left[R_{ik} \frac{\partial \bar{u}_j}{\partial x_k} + R_{jk} \frac{\partial \bar{u}_i}{\partial x_k} \right] - C_1 \frac{\epsilon}{K} \left[R_{ij} - \frac{2}{3} \delta_{ij} K \right] - C_2 \left[P_{ij} - \frac{2}{3} \delta_{ij} P \right] - \frac{2}{3} \delta_{ij} \epsilon \tag{3}$$

where, P_{ij} can be defined as [36]:

$$P_{ij} = - \left[R_{ik} \frac{\partial \bar{u}_j}{\partial x_k} + R_{jk} \frac{\partial \bar{u}_i}{\partial x_k} \right], \quad P_f = \frac{1}{2} P_{ij} \tag{4}$$

with P_f is the fluctuating energy production, ν_t represents the turbulent (eddy) viscosity, and $\sigma^k = 1, C_1 = 1.8, C_2 = 0.6$ are empirical constants. The transport equation for turbulence dissipation rate, ϵ , is expressed as follows [37]:

$$\frac{\partial \epsilon}{\partial t} + \bar{u}_j \frac{\partial \epsilon}{\partial x_j} = \frac{\partial}{\partial x_j} \left(\left(\nu + \frac{\nu_t}{\sigma^\epsilon} \right) \frac{\partial \epsilon}{\partial x_j} \right) - C^{\epsilon 1} \frac{\epsilon}{K} R_{ij} \frac{\partial \bar{u}_i}{\partial x_j} - C^{\epsilon 2} \frac{\epsilon^2}{K} \tag{5}$$

$K = \frac{1}{2} \overline{u'_i u'_i}$ is the fluctuating kinetic energy, and ϵ is the turbulence dissipation rate. The values of constants are $\sigma^\epsilon = 1.3, C^{\epsilon 1} = 1.44, C^{\epsilon 2} = 1.92$.

The Eulerian–Lagrangian approach was used to model the two-phase flow with the CFD code Ansys Fluent 2021 R1. In this technique, the gas phase was considered to be continuous by solving momentum equations, but the solid phase (discrete phase) was addressed by tracking particles through the flow field [38].

If the dispersed second phase has a low volume percentage, particle–particle interactions can be ignored. Because the particle volume fraction was less than 10^{-3} in most areas, particle interaction was insignificant, and the two-way coupling approach, which took into account particle interaction with the gas stream, was adopted in the current investigation [17]. By determining the size and density of individual particles, the Discrete Phase Model (DPM) of the Ansys Fluent CFD code was used to model particle trajectories in the Lagrangian reference frame [6, 31].

The stochastic tracking model may forecast particle dispersion owing to fluid phase turbulence. This model captures the impact of instantaneous turbulent velocity variations on particle trajectories by using stochastic techniques [39]. The Discrete Random Walk (DRW) model [40] was used in the current CFD simulation to analyze turbulent particle dispersion. The Rosin–Rammler equation was used to account for the particle size distribution. Morsi and Alexander [41] correlation is employed to estimate the drag coefficient of spherical particles in terms of relative Reynolds number (Re_p).

The particle equation of motion is defined as [42]:

$$\frac{du_{pi}}{dt} = \frac{18\mu}{\rho_p d_p^2} \frac{C_D Re_p}{24} (u_i - u_{pi}) + \frac{g_i (\rho_p - \rho)}{\rho_p} \tag{6}$$

$$\frac{dx_{pi}}{dt} = u_{pi} \tag{7}$$

where the term $\frac{18\mu}{\rho_p d_p^2} \frac{C_D Re_p}{24} (u_i - u_{pi})$ is the drag force per unit particle mass.

In Eq. (6), ρ_p and d_p represent the particle density and diameter, respectively, C_D is the drag coefficient, u_i and u_{pi} show the instantaneous gas and particle velocities, respectively. g_i is the gravitational acceleration and Re_p indicates the relative Reynolds number, which can be written as:

$$Re_p = \frac{\rho_p d_p |u - u_p|}{\mu} \tag{8}$$

where μ corresponds to dynamic viscosity.

2.2.1 Modeling of erosion

The particle effect on the wall causes erosion. The impacts of tangential erosion on the surface of swirling flows are often stronger than conventional erosion impacts on the surface [28]. The Det Norske Veritas (DNV) erosion model was utilized for modeling surface erosion in the gas cyclone which is presented in Table 2. The DNV model is a basic

Table 2 Characteristics of erosive model [28]

Erosion model of DNV						
$k = \frac{\pi^2}{2\sqrt{10}} \gamma^{\frac{5}{2}} \sqrt{\frac{1}{\rho_p} \left[\frac{1-q^2 p}{Y_p} - \frac{1-q^2 w}{Y_w} \right]^2}$						
$f(a) = 2.4647 \times 10^{-3} a + 2.9284 \times 10^{-4} a^2 - 2.1974 \times 10^{-6} a^3$						
Constant						
n	γ	ρ_p	q_p	q_w	Y_p	Y_w
1	3.1×10^6 Pa	2740 kg/m ³	0.25	0.25	4.01×10^{11} Pa	2.9×10^9 Pa

erosion model which has been widely used [43–45]. According to previous studies, the DNV erosion model is the most proper model used in several engineering fields [46, 47], particularly in gas cyclones [27–29]. Therefore, the mentioned model was employed in the current investigation. As a result, the erosion rate of the gas cyclone wall may be determined as follows [28]:

$$E^{(i)} = \dot{m}_p K f(\alpha) \left(v_p^{(i)} \right)^n \tag{9}$$

where E indicates the erosion rate; α is the contact angle; K denotes a constant associated with the physical characteristics of the wall and the particles [46, 47]; $f(\alpha)$ corresponds to the impact angle function which characterizes the surface material’s fragility and brittleness. In the DNV erosion model, parameter n represent $u'_i = u_i - \bar{u}_i$, the exponent of the exponential velocity and is a function of contact angle, whereas parameter v_p represents the particle impact velocity. Finally, the erosion is modeled from CFD data by multiplying the erosion flux by the following equation:

$$E_R = \sum_{i=1}^{np} \frac{E}{A_{face}^{(i)}} \tag{10}$$

where the erosion is expressed in the unit of mass flux (kg/m²s) [28].

2.3 Solver setting

In the present study, the finite volumes approach was used to numerically solve the governing equations of gas flow. The current modeling started with a steady solver (gas alone) for 12,000 iterations before switching to an unsteady solver (particle tracking) with a fixed time step of 10⁻⁴ s. The volume of a cyclone and the volumetric flow rate of the gas influenced the period of residence [28]. The RSTM and a standard wall function based on the strong swirl flow in a gas cyclone were used to explore the impact of turbulence [6, 48–50]. 10,000 Fly ash particles having a density of 1989.7 kg/m³ were modeled in this case. A coal-fired boiler at a power plant is injected into the square cyclone from the inlet surface with a size distribution of 1–32 μm. The inlet velocity boundary condition was given at the gas inlet region, and it was assumed that the particle and gas inlet velocity was identical. The inflow velocity ranges between 12 and 28 m/s. The hydraulic diameter was adjusted to 0.0857 m, with a turbulence intensity of 4% [38, 50, 51]. For the gas outlet, the outflow was considered. Additionally, the cyclone walls were no-slip, and the dust outflow section was adjusted to capture DPM.

Table 3 Thermo-physical characteristics [13, 39, 41, 42]

T (K)	ρ (kg/m ³)	$\mu \times 10^5$ (Pa.s)
293	1.188	1.7894
700	0.4975	3.388

Table 4 Values of PML

	Velocity (m/s)	Particle mass flow rate (g/min)		
		30	90	180
Mass loading (g/m ³)	12	6.9	20.8	41.7
	20	4.2	12.5	25.0

The SIMPLEC (semi-implicit method pressure-linked equations consistent) pressure–velocity coupling algorithm and the PRESTO (pressure staggered option) interpolation algorithm were implemented. The QUICK (quadratic upstream interpolation for convective kinetics) algorithm was used to solve the momentum equations. The turbulent kinetic energy and the dissipation rates were discretized by the second-order upwind scheme, and the Reynolds stresses were solved by the first-order upwind scheme because of the difficulty to reach the convergence in computations. The convergence errors were set as 10⁻⁵ for all equations.

Table 3 includes details on the thermophysical properties of the gas phase (air), such as viscosity and density at low and high temperatures. The temperature values were chosen to correspond to the temperature ranges reported in earlier research [13, 39, 41, 42]. The current study did not solve heat transfer, and the gas flow was supposed to be isothermal but at various temperatures. The influence of temperature-dependence of gas thermo-physical characteristics on the performance of gas cyclones, on the other hand, was investigated. In addition, six distinct PMLs with inflow velocities ranging from 12 to 20 m/s were chosen, as shown in Table 4.

2.4 Grid independence study and validation

Three distinct grid levels were used to validate the grid independence test. In the first situation, a coarse-type mesh with 480,000 elements was created. A medium-type with 720,000 elements was generated in the second case. A fine-type mesh with 1,080,000 elements was created in the third condition. The pressure profiles for three different meshes at $z/D=0.75$ are then shown in Fig. 2. Because the pressure difference between two sequential meshes was less than 1%, the computational findings proved mesh independence. As

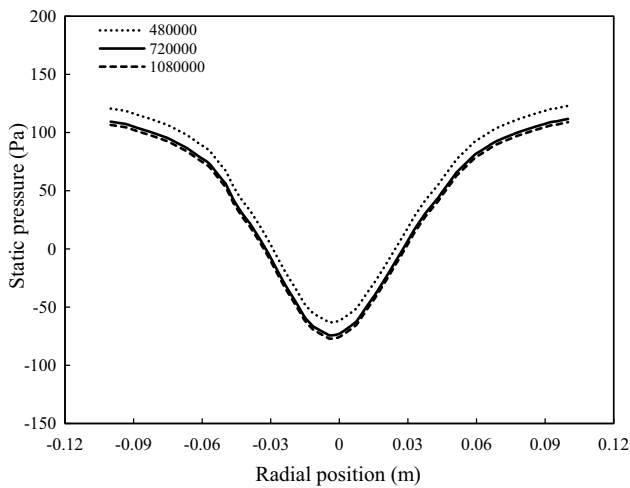


Fig. 2 Radial static pressure profiles at $v = 12$ m/s

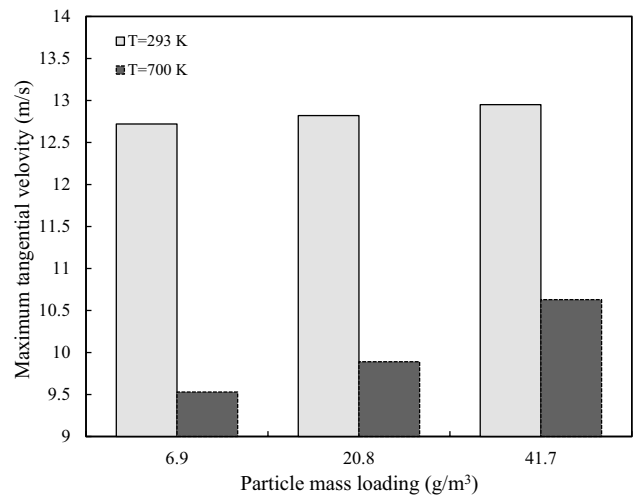


Fig. 5 Changes of the maximum tangential velocity with the PML

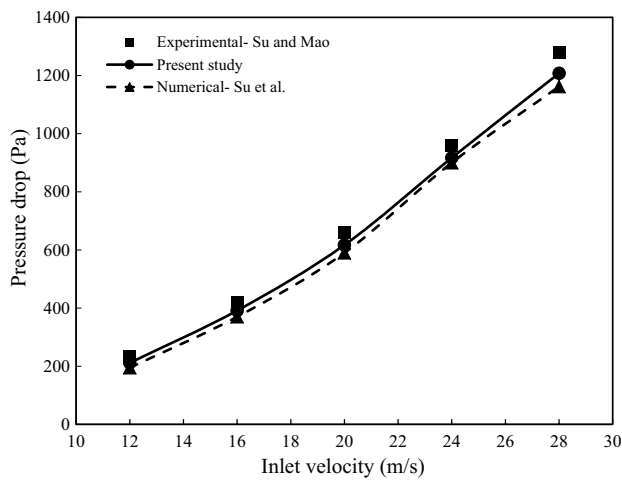


Fig. 3 Validation of pressure drop with mentioned references [3, 30]

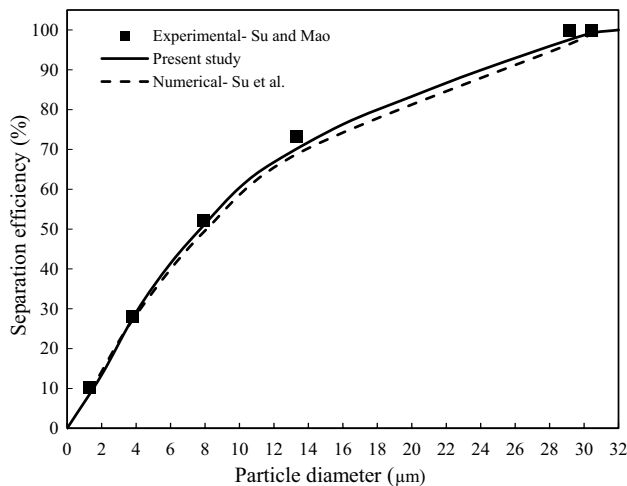


Fig. 4 Validation of separation efficiency with mentioned references [3, 30] at $v = 20$ m/s

a result, a grid with 720,000 cells (medium mesh) was used for all future numerical simulations. This mesh achieves a reasonable computational cost while retaining significant grid independence. To validate the present computational model, the results obtained were compared to Su and Mao’s [30] experimental investigation and Su et al. [3] numerical results for the square cyclone illustrated in Figs. 3 and 4. The CFD modeling conditions were chosen to be comparable to those used in prior investigations [3, 30]. The current result is consistent with experimental data and modeling results revealed in prior publications. The difference is less than 8%, which is within acceptable limits. This illustrates that the current technique is well suited for estimating the separation efficiency and other characteristics of a square cyclone.

3 Results and discussion

3.1 Tangential velocity

Figure 5 shows the relationship between the maximum tangential velocity of a square cyclone and PML at $v = 12$ m/s. It should be noted that around the interface between the inner and outer vortexes, the highest tangential velocity values have been observed [37]. The maximum tangential velocity from the time-averaged velocity field was therefore identified at an exact position below the vortex finder ($z/D = 0.75$). The PML in this study was relatively low; hence, the particle impacts on the flow field were low. The maximum tangential velocity only slightly increased when the PML was low, as seen in Fig. 6. The increase was significantly larger even though the PML increased to 41.7 g/m^3 . Maximum tangential velocity increased up to 2% for PML of 41.7 g/m^3 compared to PML of 6.9 g/m^3 .

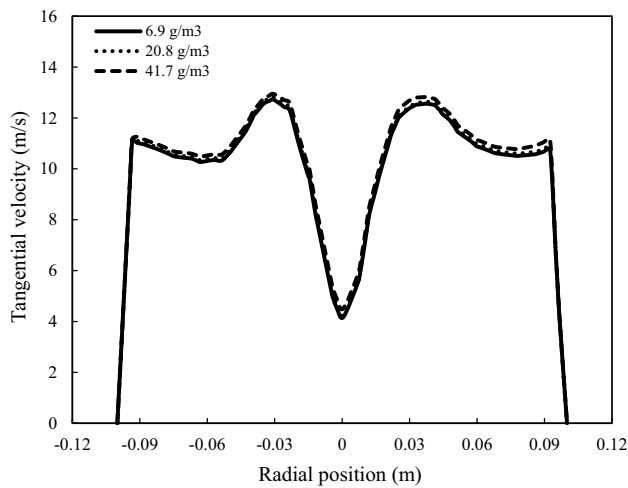


Fig. 6 Comparing the tangential velocity at different PMLs and $T=293$ K

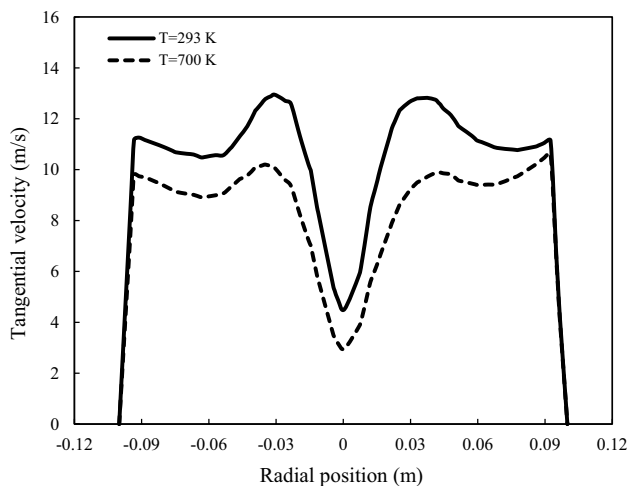


Fig. 7 Comparing the tangential velocity at different gas temperatures and PML of 41.7 g/m^3

Tangential velocity is a crucial flow parameter since it directly affects the cyclone's pressure drop and separation effectiveness. The maximum tangential velocity of all cyclones significantly reduced as the inlet temperature increased. This can be attributed to an increase in shear stress which is the result of an increase in dynamic viscosity when the inlet temperature is raised from 293 to 700 K. However, at high temperatures ($T=700$ K) compared to low gas temperatures, the increase in maximum tangential velocity caused by PML was greater. Particularly at high temperatures, any increase in PML increased maximum

tangential velocity. When compared to PML of 6.9 g/m^3 , maximum tangential velocity increased by up to 12% for PML of 41.7 g/m^3 . Greater separation efficiency is produced by higher tangential velocity [44]. As a result, at high temperatures and low PML, the square cyclone had a decreased separation efficiency.

The distributions of tangential velocity for the cyclone separator at $v=12$ m/s and $z/D=0.75$ (below the vortex finder) under varied PML and different gas temperatures are shown in Figs. 6 and 7. The tangential velocity contours for cyclones as they are influenced by PML and gas temperature are shown in Figs. 8 and 9, respectively. To evaluate the impact of gas temperature on tangential velocity, the minimum and maximum gas temperatures ($T=293$ K and $T=700$ K) were examined. The forced/free Rankine-type vortex combination was visible in the cyclone's body distribution [45]. The tangential velocity was distributed uniformly along the core axis of a cyclone. Additionally, the area between the inner and outer vortices was where the maximum tangential velocity was seen [37].

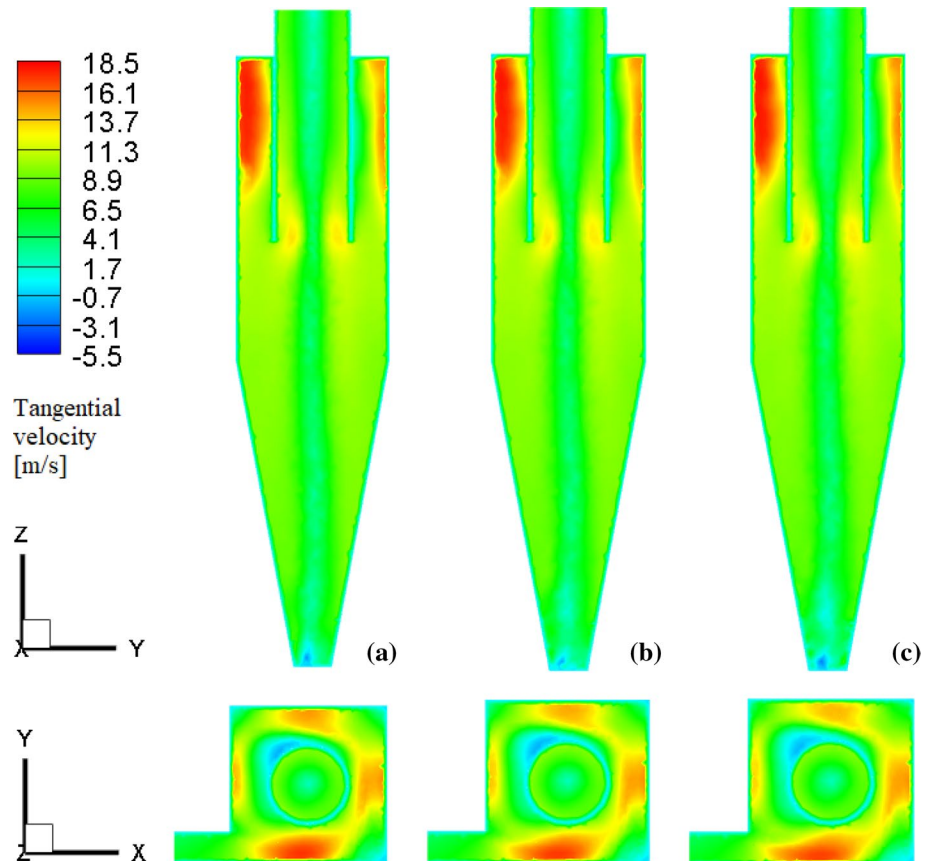
The tangential velocity distributions were demonstrated to be only slightly impacted by PML differences. While tangential velocity profiles in the free and forced vortex zones altered dramatically as PML rose, those profiles near the wall remained mostly constant. When the findings were compared, it was discovered that when the gas temperature was increased from 293 to 700 K, the tangential velocity significantly decreased. This tendency was consistent with what was discovered in other studies [42, 46]. At $T=293$ K, the maximum tangential velocity for the square cyclone with PML of 41.7 g/m^3 was around 1.1 times the inlet velocity, whereas, at $T=700$ K, it was found to be 0.9 times the inlet velocity.

3.2 Distribution of particle concentration

Particulate simulations were conducted to evaluate the categorization of particle concentration distributions. Figure 10 illustrates the distribution of particle concentration for PMLs of 6.9, 20.8, and 41.7 g/m^3 inside the square cyclone. $T=293$ K and $v=12$ m/s were used for this comparison. Three categories may be established for the particle concentration distribution. The major portion of the cyclone, which followed the gas swirling downward flow patterns, had a lower particle concentration. Because the cone radius was reduced, the gas tangential velocity increased at the conical zone of the square cyclone.

Particles were dragged toward the conical wall by the higher centrifugal force caused by the increased tangential

Fig. 8 Comparison of the tangential velocity contours under different PMLs **a** 6.9 g/m³, **b** 20.8 g/m³ and **c** 41.7 g/m³



velocity. As the conical volume reduced and the number of particles increased along the wall area, the particle concentration was higher in the conical portion of the square cyclone. Figure 10c, where the PML is noticeably bigger than in the other, makes this pattern clear. As can be observed, the particle concentration in the area along the wall increased significantly as the PML was raised. The ceiling effect, also known as the recirculation gas flow at the top portion of a cyclone with a cylindrical form, has been demonstrated in earlier research to enhance the concentration of bigger particles and, consequently, a greater particle accumulation [47, 48]. According to the current findings, the particle deposition caused a larger particle accumulation close to the top of the cyclone.

The effect of gas temperature on particle concentration distribution within the square cyclone with PML of 41.7 g/m³ and at $v = 12$ m/s is also shown in Fig. 11. At high temperatures, it is evident that fewer particles were concentrated on the bottom of the square cyclone. This is due to a weakening of the enhanced centrifugal force brought on by an

increase in gas tangential velocity, which led to fewer particles being driven in the direction of the conical wall.

To further understand how particles with varied mass loading behave, particularly below the vortex finder, Fig. 12 illustrates the radial distribution of particle concentration at the square cyclone $z/D = 0.75$ at $v = 12$ m/s. The inertia separation design idea caused the particle collection to significantly increase close to the cyclone wall. The particle concentration at the wall region (radial position = 0.095–0.1 m) increased up to six times when the PML increased from 6.9 g/m³ to 41.7 g/m³. The enhanced sweeping action of bigger particles pushed the smaller particles toward the wall zone as the PML grew, improving particle concentration at the wall zone [49]. Increased mass loading might concentrate the particles along the wall in Fig. 12 according to the current CFD results.

Figure 13 represents the impact of gas temperature on the particle concentration distribution inside a square cyclone with a PML of 41.7 g/m³ and at $v = 12$ m/s. Lower separation efficiency was caused by a considerable reduction in centrifugal force as a result of increased inlet temperature.

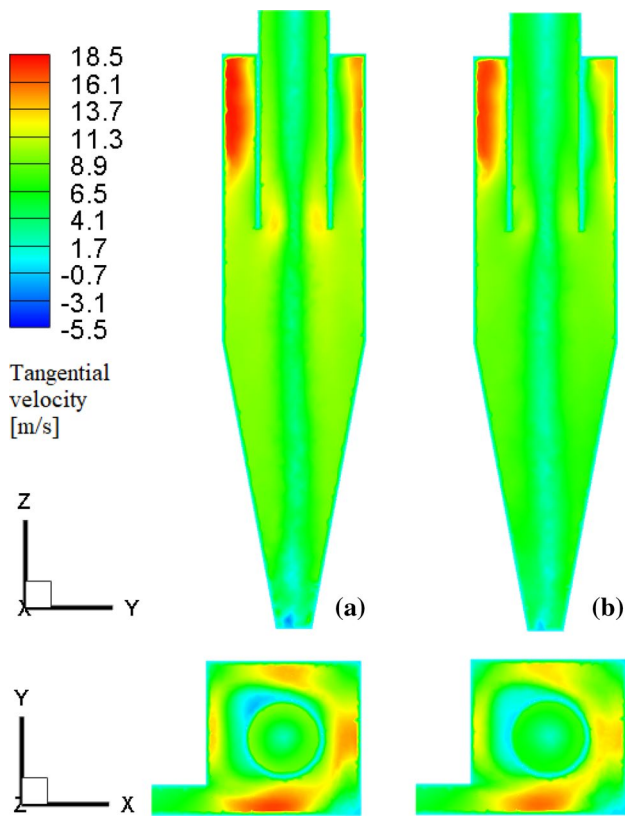
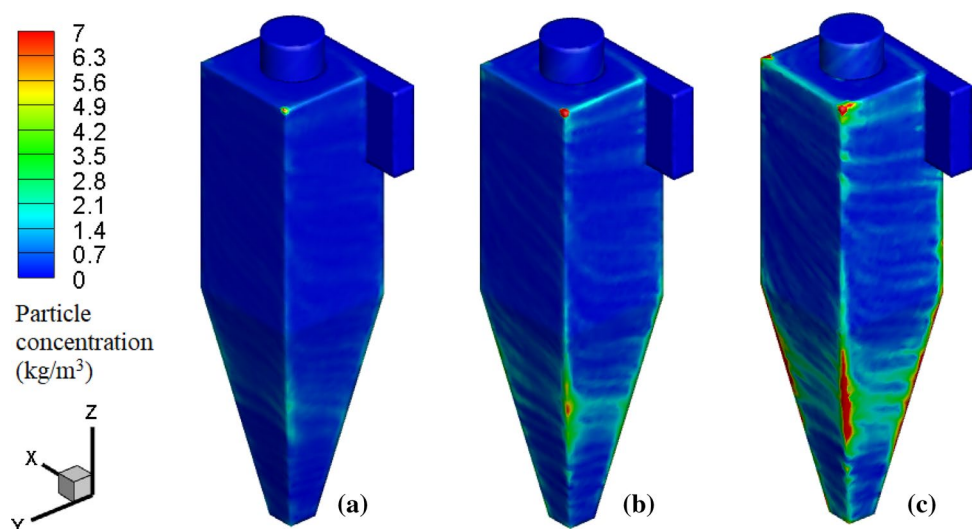


Fig. 9 Comparison of the tangential velocity contours with PML of 41.7 g/m^3 at **a** $T=293 \text{ K}$ and **b** $T=700 \text{ K}$

The more particles were pushed up against the wall and accumulated in the bottom of the cyclone at $T=293 \text{ K}$, the greater the centrifugal force.

Figure 14 demonstrates the dispersion of particle concentration along with the cyclone height at the centerline.

Fig. 10 Comparison of particle mass distribution in the gas cyclone under different mass loading **a** 6.9 g/m^3 , **b** 20.8 g/m^3 and **c** 41.7 g/m^3



The great gas swirling flow patterns that formed to progressively flow downward as the particles were transported to the conical section may have contributed to the increased particle deposition at the bottom of the square cyclone. Particle concentration at the bottom of the square cyclone rose 11 times when the PML was increased from 6.9 to 41.7 g/m^3 . Figure 15 shows the distribution of particle concentration at the centerline at low and high temperatures together with the height of the gas cyclone. This comparison was carried out at $v=12 \text{ m/s}$ and for a PML of 41.7 g/m^3 . As was already mentioned, the increase in gas temperature decreased the tangential velocity. At the bottom of the square cyclone, the particle concentration was significantly reduced as a result, by around four times.

3.3 Particle motion through the cyclone

Figure 16 shows particle movement through a cyclone separator at a velocity of 12 m/s for one second at a temperature of 293 K . This figure shows how PML affects the movement of particle clouds with sizes between 1 and $15 \mu\text{m}$. The temporal evolution changes in particle motion patterns are clearly seen in this figure. All three PMLs' particles traveled downward to the cyclone's main body, which served as the separation zone, as they entered the square cyclone. The gas was separated from the particles that had gathered on the wall's surface due to centrifugal force and those that had accumulated on the bottom due to gravity deposition.

While the various particle separation procedures are examined, it becomes clear that the larger particles ($\geq 8 \mu\text{m}$) had a stronger centrifugal force and were thus more simply separated. While the majority of the $3 \mu\text{m}$ tiny particles tried to escape via the vortex finder. The centrifugal force acting on these tiny particles, which had a diameter of $3 \mu\text{m}$, was insufficient to overcome the effect of gas drag. The main

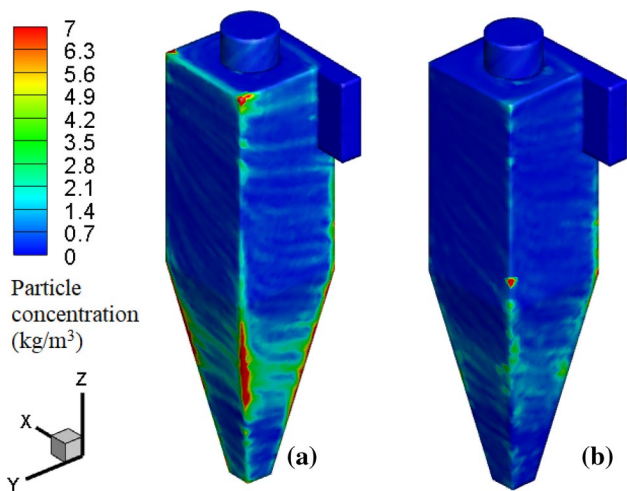


Fig. 11 Comparing the distribution of particle mass with PML of 41.7 g/m^3 at **a** $T=293 \text{ K}$ and **b** $T=700 \text{ K}$

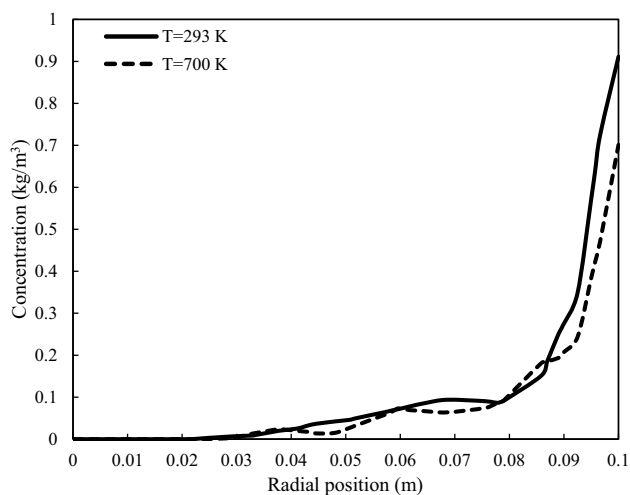


Fig. 13 Particle concentration distribution with 41.7 g/m^3 mass loading in the radial direction

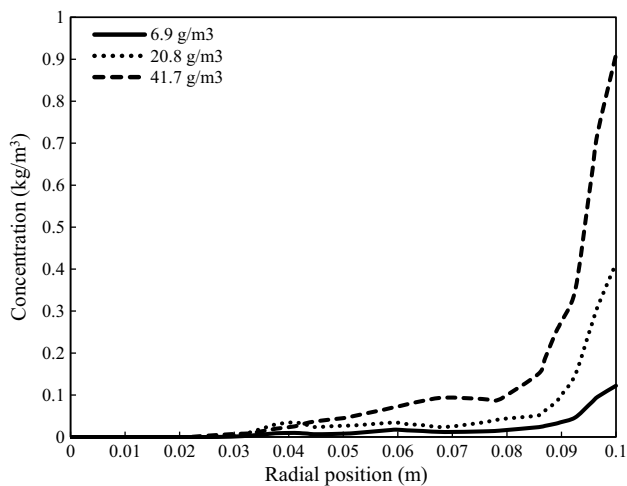


Fig. 12 Effect of PML on the distribution of particle concentration in a radial direction at $T=293 \text{ K}$

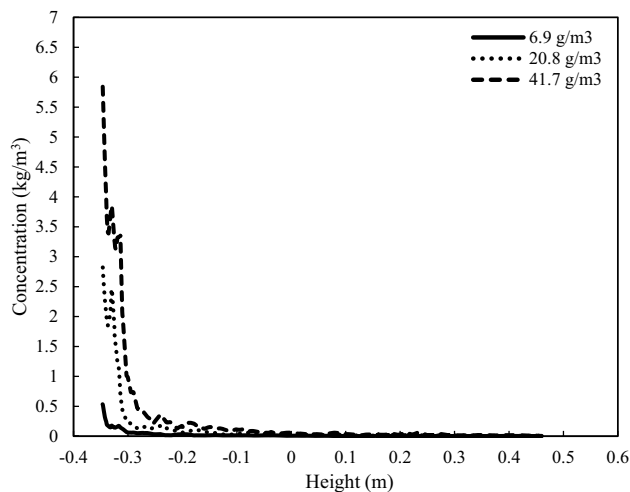


Fig. 14 Influence of PML on the distribution of particle concentration at $T=293 \text{ K}$

portion of the cyclone's top experienced a higher particle concentration due to the accumulation of bigger particles driven by the recirculation gas flow. For the first second after entering the square cyclone, this was more apparent for low PML. Some particles could not be removed from the gas as a consequence. Likewise, more particles accumulated at the conical bottom section and stayed there for a longer period as the gas tangential velocity grew with PML, increasing the likelihood that the particles would separate from one another.

Figure 17 shows the temporal history of particle clouds with a mass loading of 41.7 g/m^3 moving through square cyclones at different temperatures and $v=12 \text{ m/s}$. The bulk of the particles remained in the conical core of the square cyclone. It was envisaged that these particles would interact with the upward flow and leave the exit region. On the other hand, some of the particles were separated from the gas, and the majority of them concentrated at the bottom of the square cyclone. This is because the impact of centrifugal force was greater at 293 K .

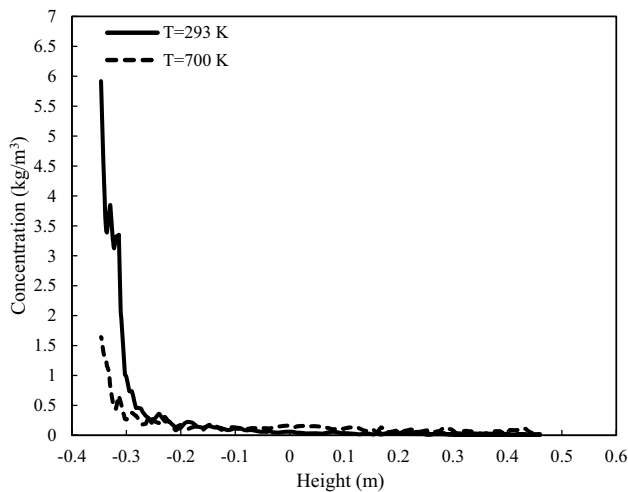


Fig. 15 Particle concentration distribution with 41.7 g/m^3 mass loading at $T=293 \text{ K}$

3.4 Particle separation efficiency

Figure 18 shows how PML affects a square cyclone's particle separation efficiency at basically two inlet velocities ($v=12 \text{ m/s}$ and $v=20 \text{ m/s}$). The DPM model was used to calculate the separation efficiency based on the collected dustbin particles, which ranged in size from 1 to $32 \mu\text{m}$. As was expected, efficiency increased as particle size increased. The load of the particle accumulation on the wall increases with particle size. By examining separation efficiencies, it was discovered that PML appeared to have different effects on cyclone efficiency at low and high inlet velocities. Enhancing the PML increased the cyclone separation efficiency at a lower inlet air velocity of 12 m/s , as shown in Fig. 18a. The fundamental reason can be attributed to the agglomeration of smaller particles and the augmentation of bigger particles with sweeping effects [49]. The PML has less of an impact on separation efficiency with the higher velocity in Fig. 18b. The substantial interaction between the smaller particle aggregations prevented the aggregation collection process at higher flow velocities. Figure 18b demonstrates a slight improvement in separation efficiency for smaller particles at higher PMLs, which is most likely caused by the sweeping motion of bigger particles.

The square cyclone operated consistently at high and low gas temperatures, as shown in Fig. 19a, b. It is clear that as

the temperature increased, separation efficiency dropped and the tangential velocity decreased. Reduced centrifugal force would also result in less particle trapping. According to a prior study [39], the maximum value of separation efficiency was determined at the lowest temperature ($T=293 \text{ K}$), while the lowest value was obtained at the highest temperature ($T=700 \text{ K}$). Additionally, when the inflow velocity rose, the separation efficiency of all square cyclones increased. The efficiency of particle separation and the centrifugal force were both improved by increasing tangential velocity [46]. When the 50% cut size was examined, it was found that as the gas temperature rose, it grew dramatically. The particle size at which the cyclone efficiency is 50% is referred to as the "50% cut size" [44]. The 50% cut size was $17.7 \mu\text{m}$ at $T=293 \text{ K}$, but it raised to $18.6 \mu\text{m}$ at $v=12 \text{ m/s}$ with a PML of 41.7 g/m^3 , which is an increase of 5%.

3.5 Pressure drop

One of the most important characteristics of a gas cyclone is pressure drop. Pressure drop is calculated using the pressure difference between the inlet and outlet sections. The pressure in the cyclone lowers due to friction between the gas flow and the wall of the cyclone and the vortex finder. Figure 20 depicts the effect of temperature on predicted pressure drop for the square cyclone at various inlet velocities ranging from 12 to 28 m/s and PML of 41.7 g/m^3 . Furthermore, an increase in inlet velocity led to a significant rise in pressure drop, this behavior is reported in previous studies [48].

CFD findings indicated that increasing the inlet temperature considerably reduced the pressure drop. This is most visible at higher inlet velocities, as swirl flow dominates throughout the square cyclone. At $v=28 \text{ m/s}$, increasing the inlet temperature (from 293 to 700 K) decreased pressure loss by approximately 36%. The reduction in pressure drop may be represented as an increase in dynamic viscosity due to a rise in the inlet flow temperature, which causes an increase in shear stress and a decrease in tangential velocity of the fluid in the cyclone body. The higher the tangential velocity of the fluid, the greater the dissipation [48], which causes a greater pressure drop at low temperatures.

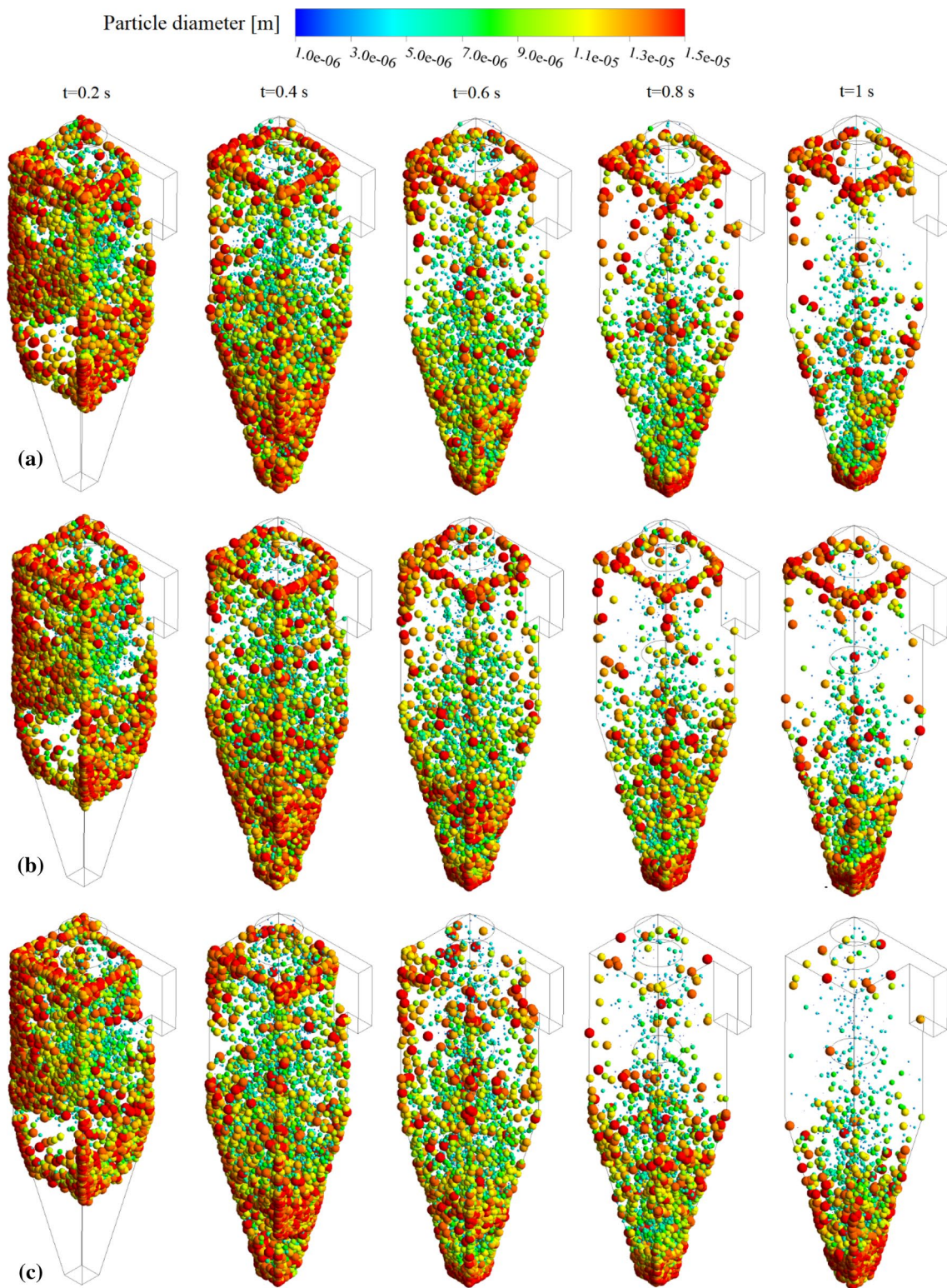


Fig. 16 Particles motion under different mass loading at $v = 12 \text{ m/s}$ **a** 6.9 g/m^3 **b** 20.8 g/m^3 and **c** 41.7 g/m^3 at $T = 293 \text{ K}$

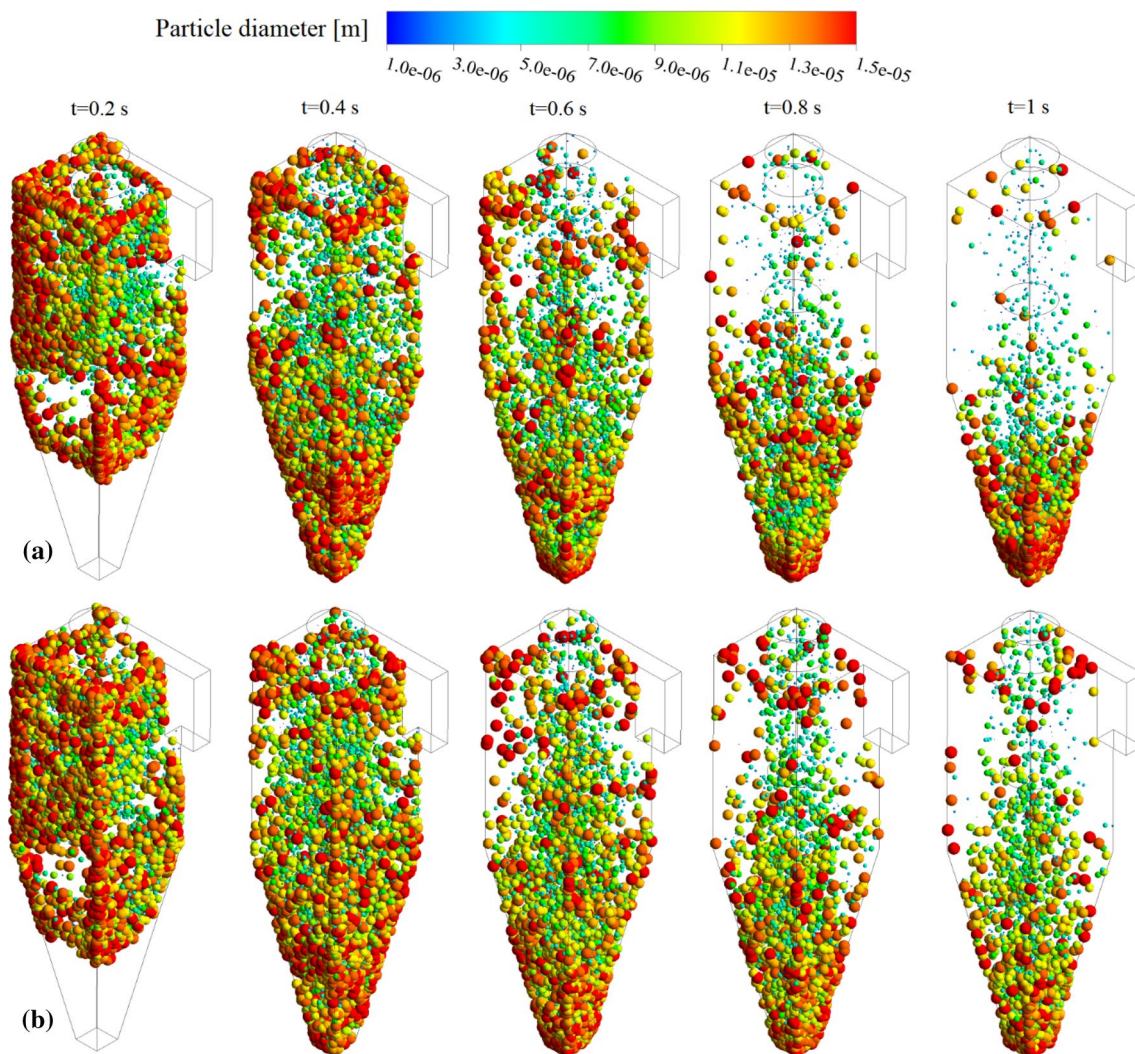


Fig. 17 Particles motion with $v = 12$ m/s at **a** low ($T = 293$ K) and **b** high temperatures ($T = 700$ K)

3.6 Erosion analysis

The present section addressed the cyclone erosion walls induced by the impact of carbon particles. As the one-way coupling was employed in the present simulations for erosion prediction, the influence of particles on the continuous phase may be ignored for low solid loadings [52, 53]. Figure 21 depicts the influence of PML on the erosion rate of a square cyclone with inlet velocities of 12 m/s and 20 m/s. It was found that as the PML augmented, so increased the

erosion rate. When PML is 41.7 g/m^3 , the maximum erosion rate is nearly four times that of PML of 6.9 g/m^3 . Furthermore, the erosion rate is greater for all PML at $v = 20$ m/s than at $v = 12$ m/s.

Figure 22 demonstrates the erosion patterns of the cyclone wall surfaces for various PMLs at $v = 12$ m/s. The erosion rate in the cone is substantially higher than in the entry and cylindrical region of the square cyclone, as predicted. This might be because of the stronger vortex created in this region in conjunction with higher negative static pressure values.

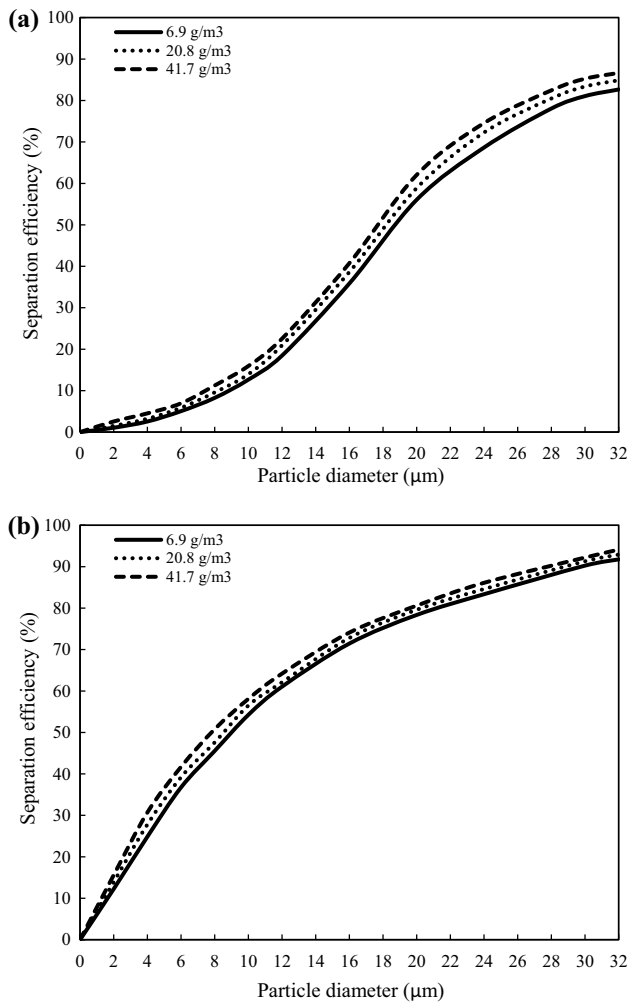


Fig. 18 Impact of PML on changes of separation efficiency versus particle size at **a** $v = 12$ m/s and **b** $v = 20$ m/s

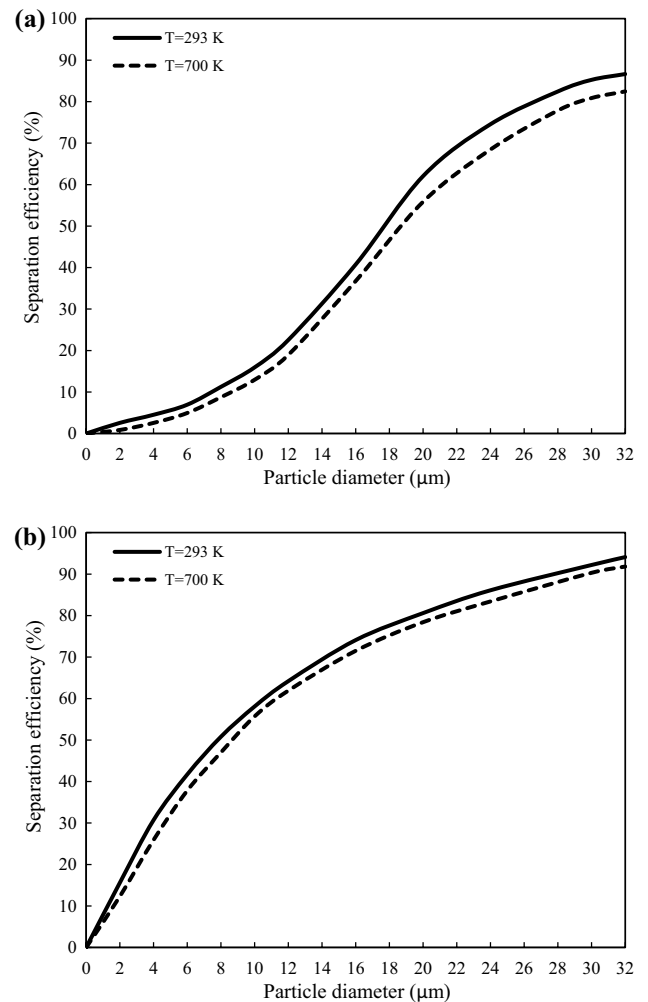


Fig. 19 Changes of separation efficiency in terms of particle size with PML of 41.7 g/m^3 **a** $v = 12$ m/s and **b** $v = 20$ m/s

Because the erosion rate distribution follows the particle trajectories, it may be argued that the particles interact with the cyclone's cone wall rather than its cylindrical section. These patterns were comparable to those described for cylindrical cyclone separators in ref. [21]. To mitigate the detrimental impacts of a high erosion rate, the cone surface should be covered with erosion-resistant materials.

4 Conclusions

The present study utilized CFD modeling to investigate the effects of PML on the internal flow field and particle separation efficiency of the square cyclone at low and high temperatures. The airflow and particle dynamics in the square cyclone were examined using the Eulerian–Lagrangian

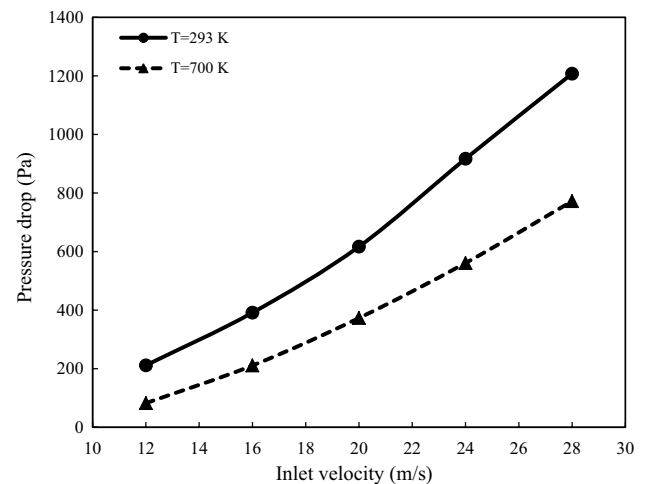


Fig. 20 Changes in pressure drop in terms of inlet velocity

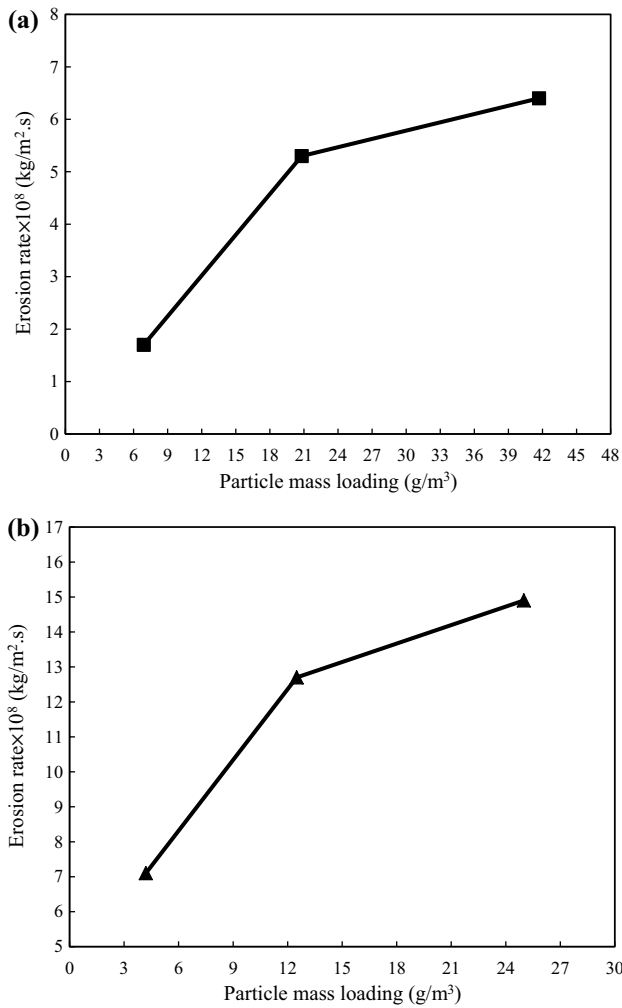
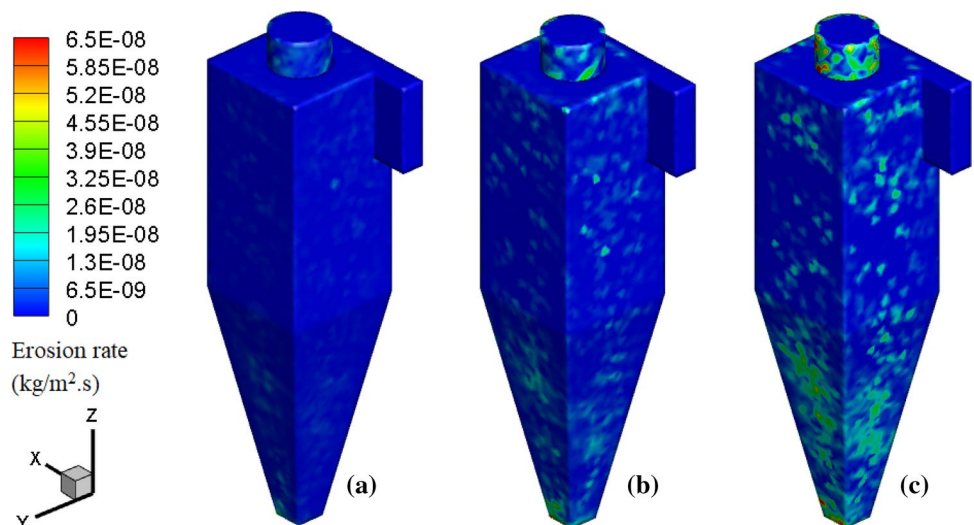


Fig. 21 Variation of highest erosion rate with the PML for **a** $v = 12 \text{ m/s}$, **b** $v = 20 \text{ m/s}$

method. The CFD simulation makes it possible to calculate the essential features of particle motion and analyze the separation efficiency. PMLs with a range of $6.9\text{--}41.7 \text{ g/m}^3$ were taken into consideration. The estimated pressure drop and separation efficiency were compared to experimental data from reference [30] and numerical findings from reference [3], which showed good agreement, to highlight the accuracy of CFD modeling.

- CFD modeling led to a better understanding of the particulate flow in the square cyclone separator.
- The flow pattern and performance of the square cyclone were influenced by both PML and gas temperature, with gas temperature having the most impact.
- When the separation processes of different particles are compared, it is apparent that the bigger particles ($8 \mu\text{m}$) were subjected to more centrifugal force and so separated more effectively. The great majority of small particles with diameters of less than $3 \mu\text{m}$ exited via the outflow section of the cyclone.
- Larger particles with lower PML aggregated near the top of the main part of the cyclone, where they could not be separated from the gas, according to observations about the motion of the particles that were compatible with the particle concentration profiles.
- With the increase in gas temperature at $v = 12 \text{ m/s}$ and PML of 41.7 g/m^3 , a 5% improvement of the 50% cut size was predicted.
- It was revealed that with the increase in inlet velocity and PML, the erosion rate was enhanced. With a PML of 41.7 g/m^3 , the maximum erosion rate was nearly four times that of a PML of 6.9 g/m^3 .

Fig. 22 Comparison of erosion rate in the gas cyclone under different mass loading **a** 6.9 g/m^3 **b** 20.8 g/m^3 and **c** 41.7 g/m^3 at $v = 12 \text{ m/s}$



References

- Safikhani H, Rafiee M, Ashtiani D (2021) Numerical study of flow field in new design cyclones with different wall temperature profiles: comparison with conventional ones. *Adv Powder Technol* 32(9):3268–3277
- Nassaj OR, Toghraie D, Afrand M (2019) Effects of multi inlet guide channels on the performance of a cyclone separator. *Powder Technol* 356:353–372
- Su Y, Zheng A, Zhao B (2011) Numerical simulation of effect of inlet configuration on square cyclone separator performance. *Powder Technol* 210(3):293–303
- Fatahian H, Fatahian E (2022) Improving efficiency of a square cyclone separator using a dipleg – a CFD-based analysis. *Iran J Chem Chem Eng (IJCCCE)* 41(2):670–681. <https://doi.org/10.30492/ijcce.2020.127666.4129>
- Fatahian E, Fatahian H, Hosseini E, Ahmadi G (2021) A low-cost solution for the collection of fine particles in square cyclone: a numerical analysis. *Powder Technol* 387:454–465
- Venkatesh S, Sivapirakasam SP, Sakthivel M, Ganeshkumar S, Prabhu MM, Naveenkumar M (2021) Experimental and numerical investigation in the series arrangement square cyclone separator. *Powder Technol* 383:93–103
- Wasilewski M, Brar LS, Ligus G (2020) Experimental and numerical investigation on the performance of square cyclones with different vortex finder configurations. *Sep Purif Technol* 239:116588
- Safikhani H, Akhavan-Behabadi MA, Nariman-Zadeh N, Abadi MM (2011) Modeling and multi-objective optimization of square cyclones using CFD and neural networks. *Chem Eng Res Des* 89(3):301–309
- Venkatesh S, Kumar RS, Sivapirakasam SP, Sakthivel M, Venkatesh D, Arafath SY (2020) Multi-objective optimization, experimental and CFD approach for performance analysis in square cyclone separator. *Powder Technol* 371:115–129
- Safikhani H, Shams M, Dashti S (2011) Numerical simulation of square cyclones in small sizes. *Adv Powder Technol* 22(3):359–365
- Fatahian H, Fatahian E, Nimvari ME (2018) Improving efficiency of conventional and square cyclones using different configurations of the laminarizer. *Powder Technol* 339:232–243
- Fatahian H, Hosseini E, Fatahian E (2020) CFD simulation of a novel design of square cyclone with dual-inverse cone. *Adv Powder Technol* 31(4):1748–1758
- Qian F, Huang Z, Chen G, Zhang M (2007) Numerical study of the separation characteristics in a cyclone of different inlet particle concentrations. *Comput Chem Eng* 31(9):1111–1122
- Chu KW, Wang B, Xu DL, Chen YX, Yu AB (2011) CFD–DEM simulation of the gas–solid flow in a cyclone separator. *Chem Eng Sci* 66(5):834–847
- Kozolub P, Klimanek A, Biłdecki RA, Adamczyk WP (2017) Numerical simulation of a dense solid particle flow inside a cyclone separator using the hybrid Euler–Lagrange approach. *Particuology* 31:170–180
- Bogodage SG, Leung AYT (2016) Improvements of the cyclone separator performance by down-comer tubes. *J Hazard Mater* 311:100–114
- Huang AN, Ito K, Fukasawa T, Fukui K, Kuo HP (2018) Effects of particle mass loading on the hydrodynamics and separation efficiency of a cyclone separator. *J Taiwan Inst Chem Eng* 90:61–67
- Derksen JJ, Sundaresan S, Van den Akker HEA (2006) Simulation of mass-loading effects in gas–solid cyclone separators. *Powder Technol* 163(1–2):59–68
- Wan G, Sun G, Xue X, Shi M (2008) Solids concentration simulation of different size particles in a cyclone separator. *Powder Technol* 183(1):94–104
- Dehdarinejad E, Bayareh M (2022) Impact of non-uniform surface roughness on the erosion rate and performance of a cyclone separator. *Chem Eng Sci* 249:117351
- Sedrez TA, Decker RK, da Silva MK, Noriler D, Meier HF (2017) Experiments and CFD-based erosion modeling for gas–solids flow in cyclones. *Powder Technol* 311:120–131
- Pereira GC, de Souza FJ, de Moro Martins DA (2014) Numerical prediction of the erosion due to particles in elbows. *Powder Technol* 261:105–117
- Wang GR, Chu F, y Tao S, Jiang L, Zhu H (2015) Optimization design for throttle valve of managed pressure drilling based on CFD erosion simulation and response surface methodology. *Wear* 338:114–121
- Jafari M, Mansoori Z, Avval MS, Ahmadi G, Ebadi A (2014) Modeling and numerical investigation of erosion rate for turbulent two-phase gas–solid flow in horizontal pipes. *Powder Technol* 267:362–370
- Chu KW, Kuang SB, Yu AB, Vince A, Barnett GD, Barnett PJ (2014) Prediction of wear and its effect on the multiphase flow and separation performance of dense medium cyclone. *Miner Eng* 56:91–101
- Chu KW, Wang B, Yu AB, Vince A (2012) Computational study of the multiphase flow in a dense medium cyclone: effect of particle density. *Chem Eng Sci* 73:123–139
- Schneiderbauer S, Haider MF, Hauzenberger F, Pirker S (2016) A Lagrangian–Eulerian hybrid model for the simulation of industrial-scale gas–solid cyclones. *Powder Technol* 304:229–240
- Parvaz F, Hosseini SH, Elsayed K, Ahmadi G (2018) Numerical investigation of effects of inner cone on flow field, performance and erosion rate of cyclone separators. *Sep Purif Technol* 201:223–237
- Foroozesh J, Parvaz F, Hosseini SH, Ahmadi G, Elsayed K, Babaoğlu NU (2021) Computational fluid dynamics study of the impact of surface roughness on cyclone performance and erosion. *Powder Technol* 389:339–354
- Su Y, Mao Y (2006) Experimental study on the gas–solid suspension flow in a square cyclone separator. *Chem Eng J* 121(1):51–58
- Elsayed K, Lacor C (2012) Modeling and Pareto optimization of gas cyclone separator performance using RBF type artificial neural networks and genetic algorithms. *Powder Technol* 217:84–99
- Yohana E, Tauviqirrahman M, Yusuf B, Choi KH, Paramita V (2021) Effect of vortex limiter position and metal rod insertion on the flow field, heat rate, and performance of cyclone separator. *Powder Technol* 377:464–475
- Elsayed K, Lacor C (2011) The effect of cyclone inlet dimensions on the flow pattern and performance. *Appl Math Model* 35(4):1952–1968
- Bogodage SG, Leung AY (2015) CFD simulation of cyclone separators to reduce air pollution. *Powder Technol* 286:488–506
- Launder BE, Reece GJ, Rodi W (1975) Progress in the development of a Reynolds-stress turbulence closure. *J Fluid Mech* 68(3):537–566
- Wang S, Fang M, Luo Z, Li X, Ni M, Cen K (1999) Instantaneous separation model of a square cyclone. *Powder Technol* 102(1):65–70
- Hoekstra AJ, Derksen JJ, Van Den Akker HEA (1999) An experimental and numerical study of turbulent swirling flow in gas cyclones. *Chem Eng Sci* 54(13–14):2055–2065
- Elsayed K, Lacor C (2010) Optimization of the cyclone separator geometry for minimum pressure drop using mathematical models and CFD simulations. *Chem Eng Sci* 65(22):6048–6058
- Safikhani H, Hajiloo A, Ranjbar MA (2011) Modeling and multi-objective optimization of cyclone separators using CFD and genetic algorithms. *Comput Chem Eng* 35(6):1064–1071

40. Elsayed K, Lacor C (2012) The effect of the dust outlet geometry on the performance and hydrodynamics of gas cyclones. *Comput Fluids* 68:134–147
41. Morsi SAJ, Alexander AJ (1972) An investigation of particle trajectories in two-phase flow systems. *J Fluid Mech* 55(2):193–208
42. Elsayed K, Lacor C (2011) Numerical modeling of the flow field and performance in cyclones of different cone-tip diameters. *Comput Fluids* 51(1):48–59
43. Veritas DN (2007) Recommended practice RP O501 erosive wear in piping systems. DNV Recommended Practice, vol 4, pp 1–43
44. Vieira RE, Mansouri A, McLaury BS, Shirazi SA (2016) Experimental and computational study of erosion in elbows due to sand particles in air flow. *Powder Technol* 288:339–353
45. Wu J, Graham LJW, Lester D, Wong CY, Kilpatrick T, Smith S, Nguyen B (2011) An effective modeling tool for studying erosion. *Wear* 270(9–10):598–605
46. Peng W, Cao X (2016) Numerical prediction of erosion distributions and solid particle trajectories in elbows for gas–solid flow. *J Nat Gas Sci Eng* 30:455–470
47. Forder A, Thew M, Harrison D (1998) A numerical investigation of solid particle erosion experienced within oilfield control valves. *Wear* 216(2):184–193
48. Fatahian H, Fatahian E, Nimvari ME, Ahmadi G (2021) Novel designs for square cyclone using rounded corner and double-inverted cones shapes. *Powder Technol* 380:67–79
49. Song C, Pei B, Jiang M, Wang B, Xu D, Chen Y (2016) Numerical analysis of forces exerted on particles in cyclone separators. *Powder Technol* 294:437–448
50. Hosseini E, Fatahian H, Ahmadi G, Eshagh Nimvari M, Fatahian E (2021) CFD study on the effect of gas temperature on the separation efficiency of square cyclones. *J Braz Soc Mech Sci Eng* 43(9):1–13
51. Wasilewski M, Brar LS (2019) Effect of the inlet duct angle on the performance of cyclone separators. *Sep Purif Technol* 213:19–33
52. Song XG, Park JH, Kim SG, Park YC (2013) Performance comparison and erosion prediction of jet pumps by using a numerical method. *Math Comput Model* 57(1–2):245–253
53. Duarte CAR, de Souza FJ, de Vasconcelos Salvo R, dos Santos VF (2017) The role of inter-particle collisions on elbow erosion. *Int J Multiph Flow* 89:1–22

Publisher's Note Springer Nature remains neutral with regard to jurisdictional claims in published maps and institutional affiliations.

Springer Nature or its licensor holds exclusive rights to this article under a publishing agreement with the author(s) or other rightsholder(s); author self-archiving of the accepted manuscript version of this article is solely governed by the terms of such publishing agreement and applicable law.